Research Article

Toru Miyake, Lei He*, Takamoto Itoh, Taiki Yamamoto and Chiaki Hisaka

Development of a piezo actuator-based fatigue testing machine for miniature specimens and validation of size effects on fatigue properties

https://doi.org/10.1515/jmbm-2024-0029
received May 08, 2024; accepted December 08, 2024

Abstract: This study presents the development of a piezo actuator-based fatigue testing machine specifically for miniature specimens. The machine's specifications include a maximum axial load of 1 kN, a maximum frequency of 15 Hz, and overall dimensions of 1,174 mm × 370 mm × 270 mm (height × length × width). Finite element analysis was employed to design two types of specimens with dimensions of 22 mm length, 8 mm width, and 2.2 mm thickness, each having a gauge length of 4 mm and diameters of 1.6 and 1.8 mm. Preliminary testing indicated that fractures initiated in the R-section of the specimen with a 1.8 mm diameter, leading to the selection of the 1.6 mm diameter specimen. To examine the influence of size on fatigue behavior, validation tests were conducted using AISI 304 and AISI 310S. Results indicated that, in the low-cycle fatigue region, size effects were negligible. However, as applied stress amplitude decreased, the fatigue life or fatigue limit of the miniature specimens surpassed that of bulk specimens.

Keywords: miniature specimen design, piezo actuator fatigue testing machine, verification tests

*** Corresponding author: Lei He,** College of Science and Engineering, Ritsumeikan University, 1-1-1 Nojihigashi, Kusatsu-shi, Shiga, 525-8577, Japan, e-mail: lei-he@fc.ritsumei.ac.jp, tel: +81-77-561-5281
Toru Miyake: Graduate School of Science and Engineering, Ritsumeikan University, Nojihigashi, Kusatsu-shi, Shiga, 525-8577, Japan; Chugai Technos Corporation, 9-12, Yokogawa-shinmachi, Nishi-ku, Hiroshima-shi, 733-0013, Japan
Takamoto Itoh: College of Science and Engineering, Ritsumeikan University, 1-1-1 Nojihigashi, Kusatsu-shi, Shiga, 525-8577, Japan
Taiki Yamamoto: Graduate School of Science and Engineering, Ritsumeikan University, Nojihigashi, Kusatsu-shi, Shiga, 525-8577, Japan
Chiaki Hisaka: Harima Workshop, Kobe Material Testing Laboratory Co. Ltd, Hyogo, 675-0155, Japan

1 Introduction

Fatigue fracture is widely recognized as a primary failure mode in in-service components and structures [1–5]. Ensuring structural integrity and establishing appropriate maintenance intervals requires precise monitoring of the operational status of these components and structures. Accurate prediction of residual strength and remaining fatigue life is crucial, especially for evaluating the service life of industrial products such as gas turbines and jet engines and assessing damage in power plants due to deterioration over time. In these scenarios, it is necessary to extract test samples from specific components or welded sections of in-service machinery and conduct static or fatigue testing to assess the degree of deterioration accurately [6,7]. However, in certain structural locations, the size required for conventional fatigue testing specimens may exceed the available sampling area, making sample extraction unfeasible. In addition, sample removal may lead to a significant decrease in performance of the original machine or result in increased repair costs. In other cases, extracting conventionally sized test specimens from structures may be impractical, such as in situations involving radioactive materials, where specimen size is constrained [8]. Therefore, the design of miniature specimens for fatigue testing is essential, allowing for minimal size while maintaining test accuracy [9–11].

Due to the challenges of conducting fatigue tests with miniature specimens, relatively few studies have been published on this topic. Li *et al.* [12] proposed a low-cycle fatigue test method at high temperatures using a miniature thin-plate specimen to investigate cyclic deformation behaviors in component materials, demonstrating that the results from miniature specimens are comparable to those obtained with standard specimens. Nozaki *et al.* [7] discussed the applicability of low-cycle fatigue testing using miniature specimens, finding that results for miniature specimens with a 1 mm diameter were similar to those of bulk specimens with a 6 mm diameter in type 304 stainless steel. Similarly, Nogami *et al.* [8] observed minimal size effects by comparing fatigue

test results between standard and four types of miniature specimens made of reduced activation ferritic/martensitic steel F82H. From these studies, it can be concluded that size effects in the low-cycle fatigue region are negligible.

In contrast, studies show that in the high-cycle fatigue region, the fatigue life of miniature specimens may exceed that of bulk specimens for EN 1.4301 acid-resistant steel [13], a common finding when investigating size effects on fatigue life. However, Kumar *et al.* [6] reached an opposing conclusion, noting that the fatigue life of miniature specimens was shorter than that of subsized specimens for 20MnMoNi55 steel. Furthermore, Volak *et al.* [14] reported complex findings from fatigue tests on five materials, comparing results from miniature and conventional specimens. For most materials, the fatigue life of miniature specimens was shorter when plotted on an *S*–*N* curve based on normal stress. However, after re-plotting the *S*–*N* curve to account for stress concentration, the fatigue life of miniature specimens for X3 steel surpassed that of conventional specimens. A similar trend was observed for other steels (X4, X5, and X7), where the fatigue life of miniature specimens was lower under normal stress conditions. Nevertheless, after adjusting applied stress amplitudes to account for stress concentration, results for X5 steel were consistent with conventional specimens in the lower fatigue life region (10^5–10^6 cycles), although opposite trends appeared in higher-cycle regions. Thus, the size effect in high-cycle fatigue is material dependent.

In general, fatigue tests for miniature specimens are typically conducted using conventional fatigue testing machines [6,12]. However, because the loading requirements for miniature specimens are significantly lower than those for conventional specimens, traditional high-capacity fatigue testing machines may not accurately control these lower loads. For example, when conducting a fatigue test with a traditional machine (maximum loading capacity of 50 kN) at an applied load of 500 N for a 2 mm diameter specimen, a control error of ±1%, which is relatively low for standard machines, would equal the target load for miniature tests, potentially causing test failure. Furthermore, for studies examining fatigue damage mechanisms using *in situ* synchrotron radiation, transportable fatigue testing machines offer greater convenience, highlighting the need for a lightweight, compact fatigue testing machine. However, as far as the authors are aware, few studies have systematically developed compact fatigue testing machines, designed miniature fatigue testing specimens, or thoroughly investigated the size effect on fatigue life. This remains an open research area.

Based on the preceding discussion, three primary objectives were proposed for this study. First, a piezo actuator-based fatigue testing machine was developed, with preliminary tests conducted to confirm output loading accuracy. Second, a miniature specimen was designed using the finite element analysis (FEA). Finally, the size effect on fatigue properties was examined by comparing fatigue test results between miniature and bulk specimens of AISI 304 and 310S.

2 Development of fatigue testing machine

2.1 Specification of fatigue testing machine

The specifications of the bidirectional piezo actuator-based fatigue testing machine developed in this study are presented in Table 1. Figure 1 shows (a) a schematic diagram, (b) an overview, and (c) magnified parts of the developed machine. The testing machine dimensions are 1,174 mm in height, 370 mm in length, and 270 mm in width. This machine uses a piezo actuator, enabling the application of tension, compression, and constant torsion loading. The control method is load-controlled, with maximum loading and displacement of ±1 kN and ±0.15 mm, respectively. In addition, once the rotation angle is set *via* torsion adjustment parts, the torsional load can be maintained at a constant value throughout the testing. The machine's maximum frequency is 15 Hz. Load measurement is carried out with a highly rigid load cell, with a maximum capacity of ±5 kN, to prevent the displacement generated by the piezo actuator from being absorbed by load cell deformation. Displacement measurement is performed using a cantilever displacement sensor, which has a maximum capacity of ±1 mm and a high responsiveness of up to 110 Hz, accommodating the machine's maximum loading frequency.

The rationale for selecting a piezo actuator as the loading mechanism is as follows. Operating without friction, the piezo actuator enables control at the nanometer level, facilitating precise fatigue testing of miniature specimens with minimal deformation. In addition, its operation is free from wear during rotation, which extends its service

Table 1: Specification of the piezo actuator-based fatigue testing machine

Size ($H \times L \times W$, mm)	1,174 × 370 × 270
Max. loading	±1 kN (axial)
Max. displacement	±0.15 mm
Max. frequency	15 Hz
Capacity of loading cell	±5 kN
Capacity of displacement measurement	±1 mm

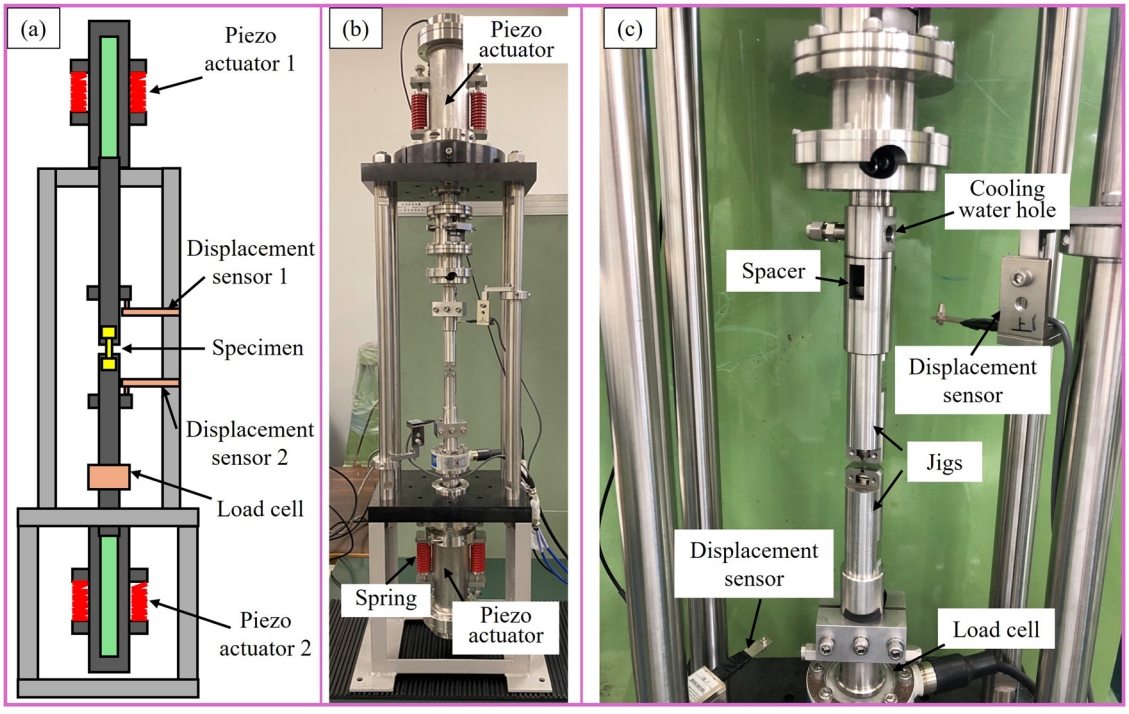

Figure 1: Appearance of fatigue testing machine: (a) schematic diagram, (b) overview, and (c) magnified parts.

life. A standalone piezo actuator can respond on the order of several kHz, making high-frequency fatigue testing feasible. Based on these advantages, a piezo actuator was chosen for this fatigue testing machine.

The control circuit diagram of the fatigue testing machine is presented in Figure 2. In this diagram, the solid arrow denotes the control signal, while the dash arrows indicate the feedback (control) and measurement signals. The control process is as follows: test conditions, such as loading amplitude and frequency, are first input into the PC, from which control signals are transmitted to LabVIEW (2019 version, National Instruments Corporation, USA). These command signals are then sent as control signals from LabVIEW to each piezo actuator through the respective drivers. The piezo actuators expand and contract in response to the command signals. Three measurement signals – loading, Displacement 1, and Displacement 2 – are subsequently sent back to LabVIEW. Notably, the loading signal also functions as a feedback signal. Based on this feedback, LabVIEW generates a new command signal that is transmitted to each piezo actuator through the corresponding actuator.

2.2 Testing frequency

To minimize testing time, it is preferable to maximize the testing frequency without compromising the test results. Therefore, this section examines the frequency characteristics of the developed fatigue testing machine.

The evaluation method involved varying the testing frequency across different loading levels to assess whether the loading control and displacement responses were consistent, based on measured loading and displacement data. To verify output loading, the load–time graph and

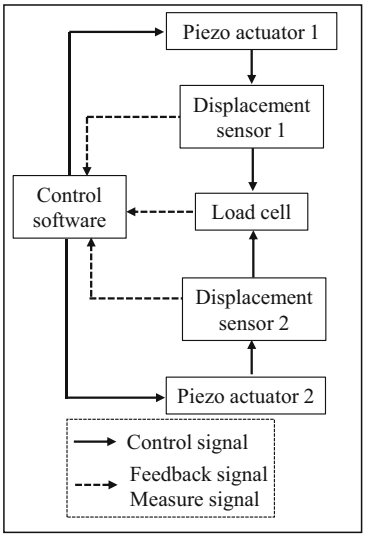

Figure 2: Control flow of the alternate piezo actuator type fatigue testing machine.

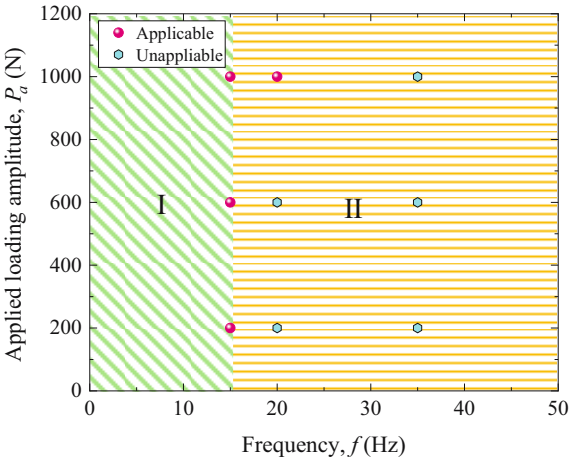

Figure 3: Frequency characteristics of the alternate piezo actuator-based fatigue testing machine.

frequency data were used to confirm whether output values reached the intended targets. In addition, abnormal vibrations, such as resonance, were evaluated by analyzing the relationship between the two displacement measurements obtained from the displacement sensors. Displacement 1 represents the upper rod displacement, while Displacement 2 indicates the lower rod displacement (Figure 1). The results of the frequency characteristic analysis are shown in Figure 3, where the horizontal axis represents the frequency f and the vertical axis shows the loading amplitude P_a. For the verification tests, frequencies of 15, 20, and 35 Hz, along with loading amplitudes of 200, 600, and 1,000 N, were used. In Figure 3, Range I represents test conditions where the machine operated normally, while Range II represents conditions where normal operation was not achieved except for one test condition. As shown, the output loads met target values for all conditions at a frequency of f = 0–15 Hz. However, at frequencies of f = 16–35 Hz, the output load only met target values for the condition of f = 20 Hz and a loading amplitude of P_a = 1,000 N. The inability to sustain target loading beyond this frequency range was attributed to resonance in the lower rod, which became more pronounced at frequencies exceeding 20 Hz. Figure 4 provides an example of a specimen tested under an applied load of 200 N at a frequency of 20 Hz. The variation in output load with the increasing number of cycles is shown in Figure 4(a), where it is observed that the output load remained stable. In addition, Figure 4(b) shows the maximum and minimum displacement values for the upper and lower rods. For the upper rod (purple plots), although some scatter is noted, the maximum and minimum values remained within ±0.03 mm, indicating controlled displacement within measurement accuracy. Conversely, displacement in the lower rod exhibited considerable scatter approximately between 2,000 and 5,000 cycles, which was attributed to resonance. Therefore, the maximum applicable frequency for the developed fatigue testing machine was determined to be f = 15 Hz.

2.3 Controlling system

The control software was developed in-house using LabVIEW. Real-time display of various measured values and graphs provides a clear view of test status during operation. The displayed information includes the current, maximum, minimum, range, and average values for loading, Displacement 1 (upper rod displacement), and Displacement 2 (lower rod displacement). In addition, the control software displays graphs showing the displacement–loading

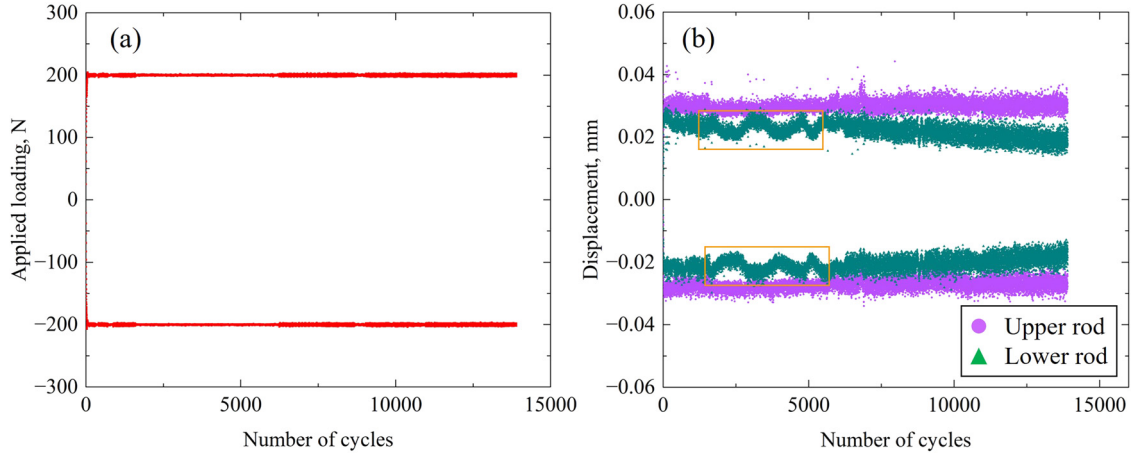

Figure 4: Variation of output values with increasing number of cycles: (a) applied loading and (b) displacement of rods.

relationship and the load variation over time. The system also features automatic load control to maintain the target value, minimizing the risk of specimen deformation due to excessive load during the attachment process.

PID control can be customized by adjusting the gain values. Currently, the test operates under proportional (*P*) control, with the integral (*I*) and differential (*D*) values set near zero. This configuration was selected due to the high responsiveness of the piezo actuator (a single piezo actuator responds on the order of kHz), as employing PI control would likely result in oscillations.

3 Specimen design and chucking jigs

3.1 Specimen design

The specimen was designed using the FEA described below. Figure 5 shows the shape and dimensions of specimen. The gauge section was designed into a cylindrical shape with a diameter of 1.6 mm to enable multiaxial loading such as axial and torsional loadings. The length of the gauge section is limited to 4 mm, because when the length of the gauge section is three times or more than its diameter, there is a risk that deflection will occur during lathe machining, which may affect surface roughness and parallelism. In addition, in consideration of sampling specimen from actual structures or components, the thickness of gripping portion is limited at 2.2 mm.

3.2 Chucking jigs

The miniature specimen must be rigidly secured to prevent irregular loading from affecting the jig during fatigue testing. Given the small size of the specimen, precise alignment of the axis is essential. To meet these requirements, a specialized holding jig was developed, as shown in Figure 6. This jig prevents impact loading during testing by applying fixing force to the specimen's end face and automatically aligns the axis between the jig and the specimen along the R-section. As illustrated in Figure 7, taper blocks A and B are adjusted by sliding bolts, which apply fixing force by pushing in a fixing rod. The specimen is further stabilized in the thickness direction by positioning it between spacers.

3.3 Conditions of FEA

In general, the specimen design aims to maximize the von Mises equivalent stress within the gauge section. However, if the specimen has a round gauge section and a square grip section, it may fracture at the corner during fatigue testing. This can occur due to surface roughness from corner machining and the direct loading contact with the jig. A preliminary test was performed with pull–push loading at an amplitude of 250 MPa using a specimen with the same dimensions as shown in Figure 5 but with a diameter of 1.8 mm. Although this specimen was designed to maximize von Mises stress at the gauge section,

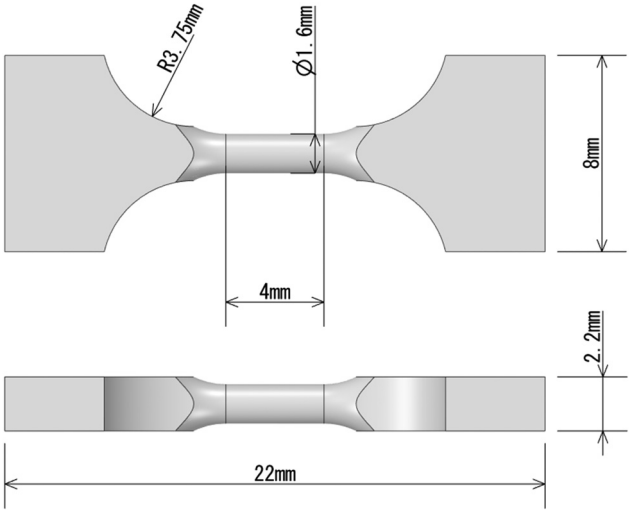

Figure 5: Shape and dimensions of specimen (mm).

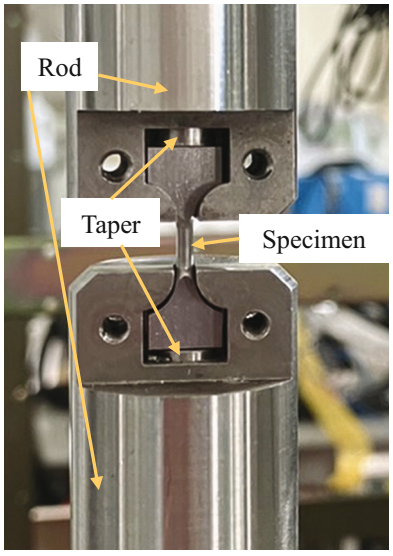

Figure 6: Photograph of gripping jig and specimen.

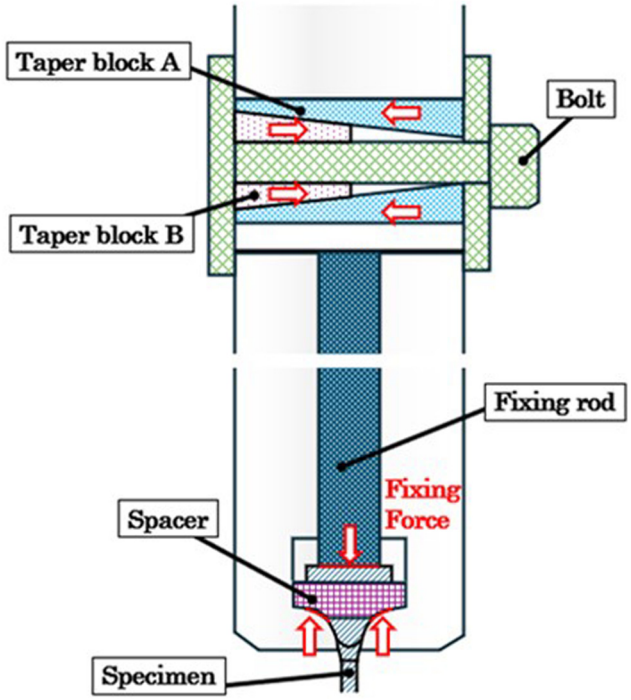

Figure 7: Schematic of the jig used for fixing the specimen.

it ruptured at the R-section, as illustrated in Figure 8(a). Conversely, in a preliminary test with a specimen diameter of 1.6 mm, the fracture occurred at the gauge section, as shown in Figure 8(b). This indicates that the design should not only maximize von Mises stress at the gauge section but also ensure that corner stress is sufficiently lower than that at the gauge section.

Based on these findings, FEA was conducted on two specimen types with gauge diameters of 1.6 and 1.8 mm. The purpose of the analyses was to determine the maximum von Mises equivalent stress at the gauge section and to compare the corner stresses to establish a required safety margin. ANSYS 2021 R2 was used for the analysis.

In the model, a half-symmetrical shape was constructed to leverage symmetry. To account for the jig's pressure at the R-section, the specimen holding jig was included in the model. The analytical shape is shown in Figure 9, and Table 2 displays the connection settings between the components. The "Contact" setting was applied to model the potential separation between the test specimen and jig under combined tensile–torsion loading. This setting prevents penetration when the distance between the components decreases, ensuring that compressive loads are transmitted, while treating separated components as if no load is transmitted. In addition, the spacer and fixing rod were modeled as bonded to the jig. The specimen's pressing force was simulated by applying initial stress along the axial (X) direction to the fixing rod, which in turn compresses the specimen against the jig, generating compressive stress at the R-section.

The material constants are presented in Table 3, and the loading boundary conditions are depicted in Figure 10. The analysis was conducted in two steps: in Step 1, the

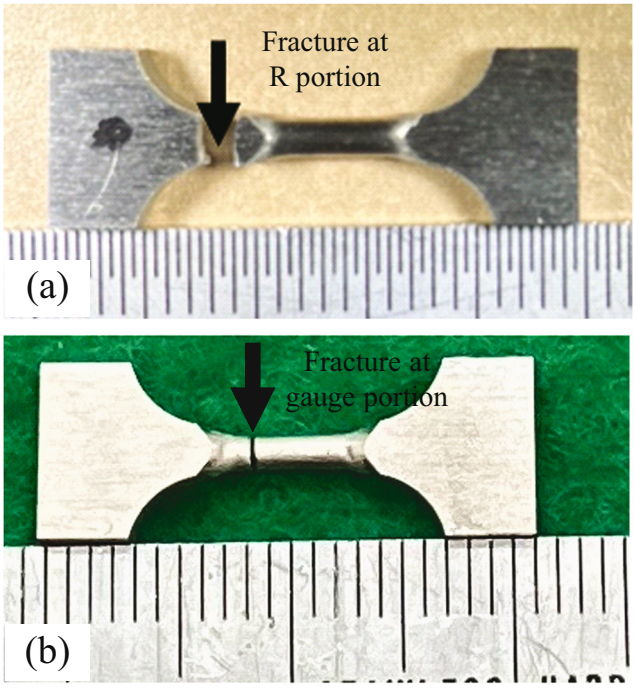

Figure 8: Fracture location for specimens with diameters of (a) 1.8 mm at the R-section and (b) 1.6 mm at the gauge section.

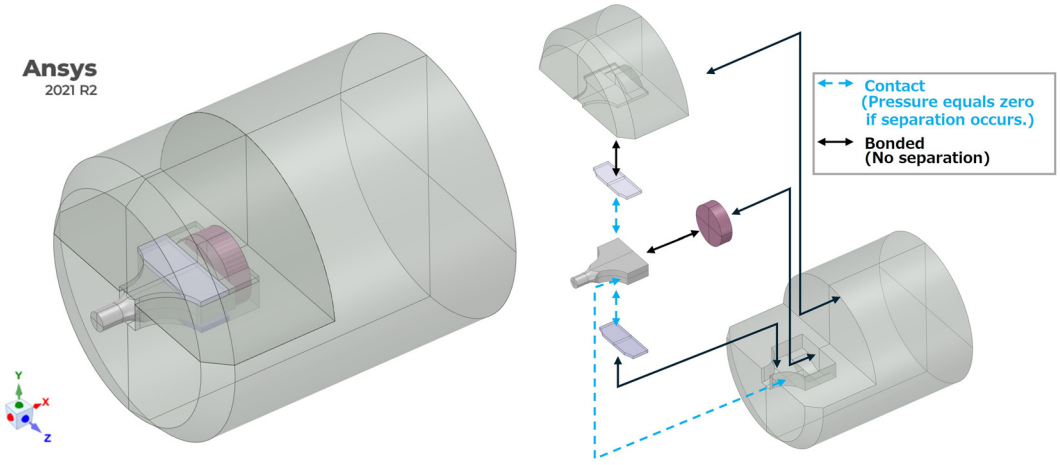

Figure 9: Overview of analysis model.

pressing load was applied, followed by the axial load in Step 2. The axial load was set at 200 MPa for the gauge section, and the fixing load was set at 1.5 times the axial load to ensure secure attachment.

4 Results and discussion

4.1 FEA

The FEA results for specimens with diameters of 1.6 and 1.8 mm are illustrated in Figure 11, using von Mises equivalent stress as the metric. Maximum von Mises stresses were observed at both ends of the gauge section for both specimen sizes, with stress differences from the gauge section remaining within 10%. Similar stress differences at the ends of the gauge section are common in non-miniature fatigue specimens and do not typically pose issues for testing. Pretests confirmed that this miniature fatigue specimen could also be tested without complications, as evidenced by the absence of fractures at the ends of the parallel section as shown in Figure 8(b).

In the R-section where fractures occurred in the pretest for the 1.8 mm specimen, the stress reached 145.3 MPa (72.6% of the gauge stress). In contrast, for the 1.6 mm diameter specimen, the R-section stress was 114.1 MPa (57.1% of the gauge stress), achieving a stress reduction of over 15%. The maximum stress at the R-section was concentrated at the edge, where the specimen interfaces with the jig, resulting in compressive stress at this contact point. Given the sharp geometry of the edge, this region becomes susceptible to crack initiation. During the pretest of the 1.8 mm specimen, high stress – exceeding 70% of the gauge stress – developed at the R-section edge, promoting crack growth and leading to early failure at the R-section before the gauge section. Although polishing the edges could potentially reduce crack formation, this is not entirely reliable, as the edges remain in contact with the jig. Consequently, reducing the stress ratio in the R-section is essential. For the 1.6 mm diameter specimen, concentrating stress in the gauge section allows for a reduced stress ratio in the R-section. Based on pretest findings, fractures initiated from the R-section for the 1.8 mm diameter specimen but from the gauge section for the 1.6 mm diameter specimen. Therefore, to avoid premature fracture, the stress at the R-section edge should remain below 57.1% of the gauge stress.

Table 2: Connection settings for component combinations

Combinations		Setting
Specimen	Jig 1	Contact
Specimen	Spacer 1	Contact
Specimen	Spacer 2	Contact
Jig 1	Jig 2	Bonded
Spacer 1	Jig 1	Bonded
Spacer 2	Jig 2	Bonded
Fixing rod	Jig 1	Bonded
Fixing rod	Specimen	Bonded

Table 3: Material constants

Material	*E* (GPa)	*v*	Part
SS400	206	0.3	Specimen
SUS310S	205	0.29	Jigs & spacer

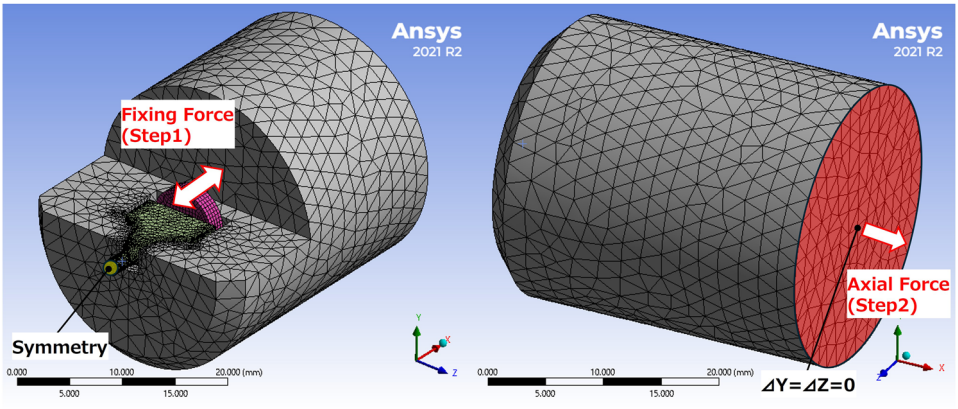

Figure 10: Boundary conditions used for analysis.

To verify the stress distribution for a specimen with a 1.6 mm diameter under combined axial–torsional loading, FEA was conducted. The magnitude of torsional loading was adjusted so that the von Mises stress in the gauge section equaled the axial loading stress (200 MPa). The developed fatigue testing machine allows for cyclic axial loading while maintaining constant torsional loading, so the analysis followed the sequence: Step 1 (pressing load) ⇒ Step 2 (shear load) ⇒ Step 3 (axial load in tension). The resulting stress distribution behaviors are shown in Figure 12. In this analysis, the R-section stress reached 116.0 MPa, approximately 41% of the gauge section stress, which was 282.8 MPa. Even under combined axial–torsional loading, the gauge section is expected to fracture at the R-section. Comparing this result with Figure 11(b) indicates that the addition of torsional loading further reduces the stress ratio

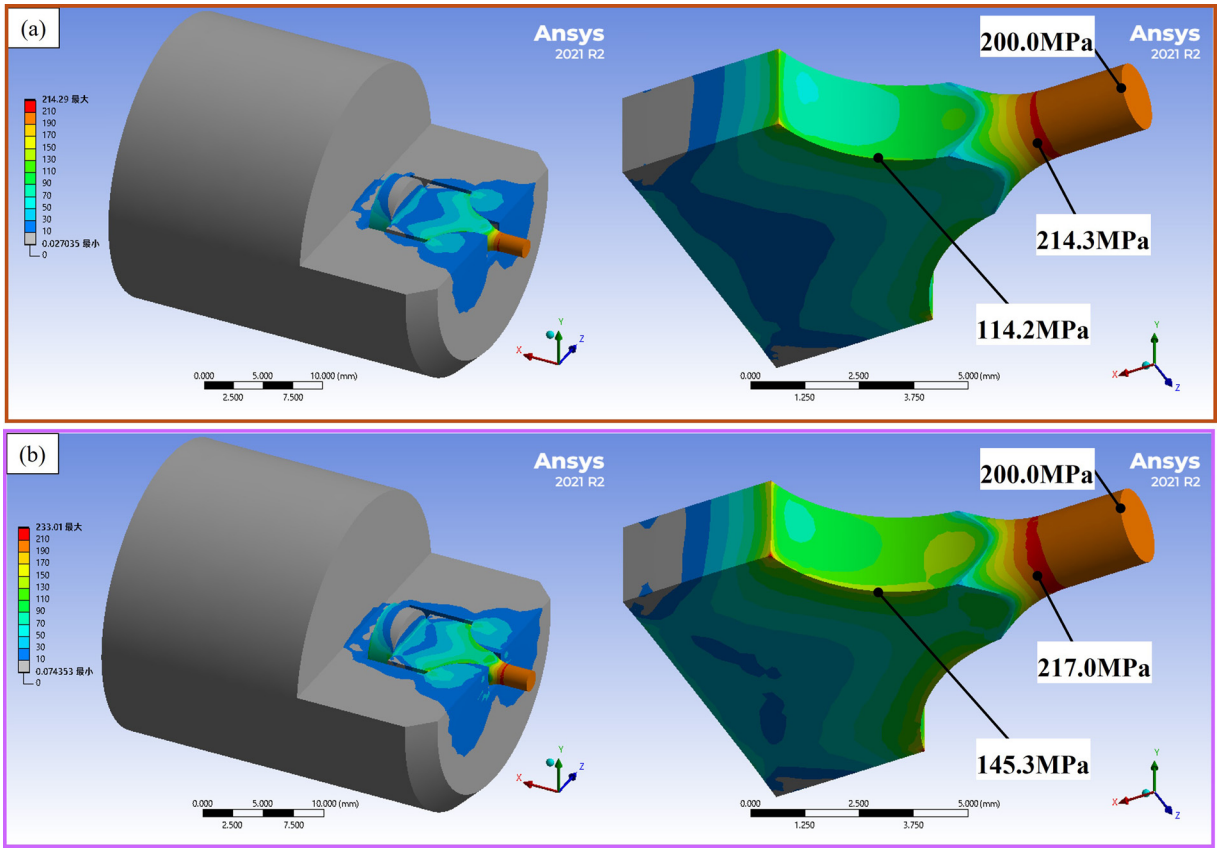

Figure 11: FEA results under axial loading for specimens with diameters of (a) 1.6 mm and (b) 1.8 mm.

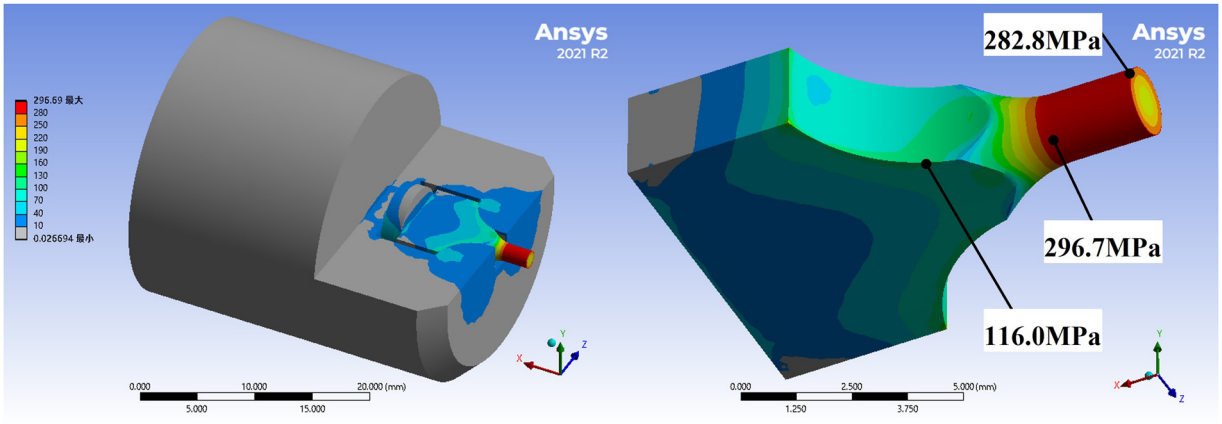

Figure 12: FEA results under combined loading for the specimen with a diameter of 1.6 mm.

in the R-section, significantly lowering the likelihood of fracture in this area compared to purely axial loading conditions (without torsion). Based on these results, the probability of fracture occurring in the gauge section remains higher than in the R-section, even under combined axial–torsional loading conditions.

4.2 Verification testing

Verification testing was conducted to investigate the size effect on fatigue life using AISI 304 and AISI 310S. Figure 13 presents a comparison of fatigue life for AISI 304 between miniature and bulk specimens, with additional data from the National Institute for Materials Science (NIMS) [15,16] included for reference. Arrows in Figure 13 indicate specimens that did not fail. At an applied stress amplitude of 300 MPa, the fatigue life of miniature specimens is slightly longer than that of bulk specimens. In contrast, at a lower stress amplitude of 270 MPa, the fatigue life difference between the two specimen types is over an order of magnitude, indicating a clear size effect. Due to the absence of fatigue limit data for bulk specimens, NIMS data were utilized for further analysis. The fatigue limit for miniature specimens is approximately 270 MPa, while the NIMS data indicate a fatigue limit of about 235 MPa for bulk specimens, lower than that of the miniature specimens. Therefore, the size effect is evident in both finite and infinite fatigue life ranges. Additionally, after normalizing the ordinate by tensile strength (σ_{UTS} of current AISI 304 is 618 MPa

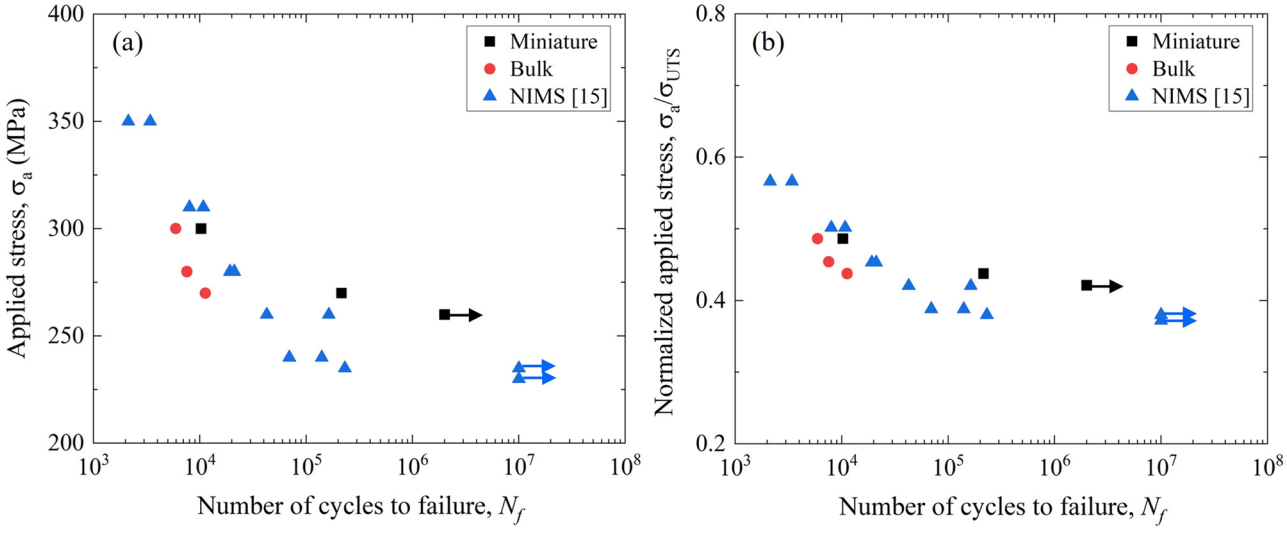

Figure 13: Comparison of fatigue life for AISI 304 between miniature and bulk specimens: (a) conventional *S–N* curves and (b) *S–N* curves normalized by tensile strength.

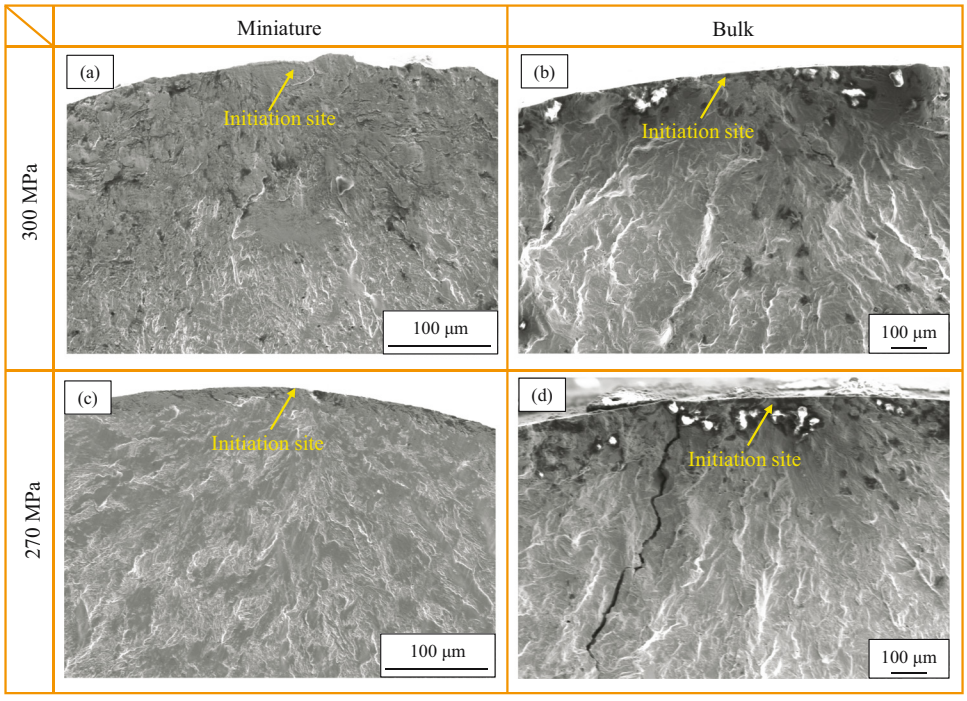

Figure 14: Fracture surface observations for (a) and (c) miniature, and (b) and (d) bulk specimens.

and σ_{UTS} of NIMS AISI 304 is 617 MPa), the gap between the NIMS data and current results narrows. It is well established that even materials from the same manufacturer and batch may show data scatter, making slight inconsistencies unavoidable.

To further investigate whether the size of the fatigue initiation site influences fatigue life for the two specimen types, fracture surface observations were performed. Typical fracture surfaces are shown in Figure 14. As depicted, fatigue cracks initiated from the surface in both specimen types, under both high and low applied stress amplitudes of 300 and 270 MPa. These observations are consistent with those obtained for bulk AISI 316 in the high-cycle regime [17,18]. Thus, while specimen size impacts fatigue life and the fatigue limit, it has minimal effect on fatigue crack initiation behavior.

In addition, the fatigue test results for AISI 310S miniature specimens, along with data from NIMS data sheets, are shown in Figure 15. At relatively high stress levels (320–400 MPa), the fatigue life of both specimen types is

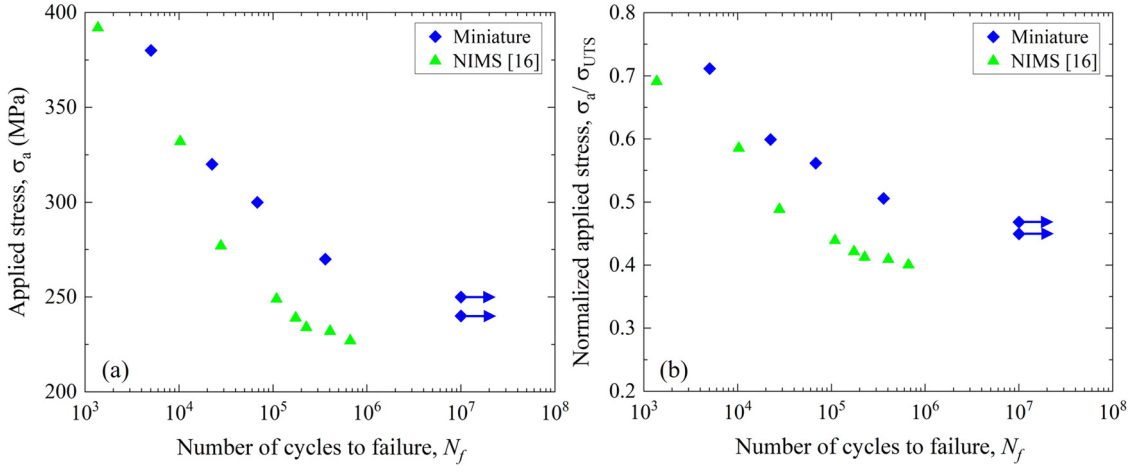

Figure 15: Comparison of fatigue life for AISI 310S between miniature and bulk specimens: (a) conventional *S–N* curves and (b) *S–N* curves normalized by tensile strength.

nearly equivalent, despite some data scatter. However, as the applied stress amplitude decreases, the fatigue life gap between the two specimen types widens significantly. While NIMS data do not include a specific fatigue limit, the trend of the *S*–*N* curve suggests an approximate fatigue limit of 200–220 MPa. In contrast, the fatigue limit of miniature specimens is around 250 MPa. Moreover, after normalizing the ordinate by tensile strength (σ_{UTS} of current AISI 310S is 534 MPa and σ_{UTS} of NIMS AISI 310S is 567 MPa), the gap at relatively high stress levels became larger, while at relative low stress levels the trend hardly changed. Based on these results, it can be concluded that a size effect is present in both materials studied, with the fatigue limit of miniature specimens exceeding that of bulk specimens. In austenitic stainless steel, fatigue cracks typically initiate at the surface from a "weak" grain in the high-cycle fatigue region. Larger-diameter specimens are more likely to contain such weak grains, which may increase the likelihood of crack initiation compared to smaller specimens [19]. This contributes to the observed size effect.

5 Conclusions

This study aimed to develop a piezo actuator-based fatigue testing machine to evaluate the remaining fatigue life of specimens taken from service components or structures. In addition, a miniature fatigue specimen was designed using FEA, and verification tests on the effect of specimen size on fatigue behavior were conducted with AISI 304 and AISI 310S stainless steel. The key conclusions are summarized as follows:

- Due to its high displacement resolution, responsiveness, and durability, a piezo actuator was selected as the power source for the developed machine. The full dimensions of the machine are 1,174 mm × 370 mm × 270 mm ($H \times L \times W$), and it allows for combined axial loading and constant torsional loading. The control system, developed in LabVIEW, includes PID control capabilities. Pretest results confirmed that the maximum applicable frequency is 15 Hz; at higher frequencies, resonance in the lower rod prevents the output load from matching the set load.
- Specimens with dimensions of 22 mm in length, 8 mm in width, 2.2 mm in thickness, a gauge length of 4 mm, and diameters of 1.6 mm and 1.8 mm were designed using FEA. For the 1.8 mm diameter specimen, stress in the R-section reached 145.3 MPa (72.6% of the gauge stress), while for the 1.6 mm specimen, it was 114.1 MPa (57.1% of the gauge stress), achieving a stress reduction of over 15%. Pretest results indicated fracture initiation in the R-section of the 1.8 mm specimen, leading to the selection of the 1.6 mm specimen for further testing.
- Verification tests with bulk and miniature AISI 304 specimens indicated that in the shorter fatigue life range, size effects on fatigue life are minimal. However, as the applied stress amplitude decreased, the gap in fatigue life or fatigue limit between bulk and miniature specimens widened. Fracture morphology was nearly identical for both specimen types, suggesting that specimen size has minimal influence on fatigue crack initiation behavior.
- Verification tests and literature data on AISI 310S specimens indicated that size effects in the low-cycle fatigue region (~10^4 cycles) were minimal. However, as stress amplitude decreased, the fatigue life of miniature specimens exceeded that of bulk specimens, confirming a notable size effect in the longer fatigue life region.

Funding information: Authors state no funding involved.

Author contributions: Toru Miyake: data curation, investigation, methodology, writing – original draft; Lei He: methodology, writing – review & editing; Takamoto Itoh: resources, supervision, review & editing; Taiki Yamamoto: investigation and experiment; Chiaki Hisaka: investigation and methodology. All authors have accepted responsibility for the entire content of this manuscript and approved its submission.

Conflict of interest: Authors state no conflict of interest.

Data availability statement: All data generated or analyzed during this study are included in this published article.

References

[1] Theil N. Fatigue life prediction method for the practical engineering use taking in account the effect of the overload blocks. Int J Fatigue. 2016;90:23–35.
[2] Hou SQ, Cai XJ, Xu JQ. A life evaluation formula for high cycle fatigue under uniaxial and multiaxial loadings with mean stresses. Int J Mech Sci. 2015;93:229–39.
[3] Tian H, Liaw PK, Strizak JP, Mansur LK. Effects of mercury on fatigue behavior of Type 316 LN stainless steel: application in the spallation neutron source. J Nucl Sci Technol. 2003;318:157–66.
[4] Colin J, Fatemi A. Variable amplitude cyclic deformation and fatigue behaviour of stainless steel 304L including step, periodic, and random loading. Fatigue Fract Eng Mater Struct. 2010;33:205–20.

[5] He L, Akebono H, Sugeta A, Hayashi Y. Cumulative fatigue damage of stress below the fatigue limit in weldment steel under block loading. Fatigue Fract Eng Mater Struct. 2020;43:1419–32.
[6] Kumar K, Madhusoodanan K, Singh RN. Miniature test techniques for life management of operating equipment. Nucl Eng Des. 2017;323:345–58.
[7] Nozaki M, Sakane M, Fujiwara M. Low cycle fatigue testing using miniature specimens. Int J Fatigue. 2020;137:105636.
[8] Nogami S, Itoh T, Sakasegawa H, Tanigawa H, Wakai E, Nishimura A, et al. Study on fatigue life evaluation using small specimens for testing neutron-irradiated materials. J Nucl Sci Technol. 2011;48(1):60–4.
[9] Nogami S, Hisaka C, Fujiwara M, Wakai E, Hasegawa A. High temperature fatigue life evaluation using small specimen. Plasma Fusion Res. 2017;12:1–6.
[10] Ma Z, Zhang B, Song Z, Liu H, Zhang G. Evaluation of the low-cycle fatigue life of thin dual-phase steel sheets for automobiles using miniature specimens. Steel Res Int. 2019;90:1900186.
[11] Sarkar R, Ray KK. Estimation of fracture toughness using miniature chevron-notched specimens. Fatigue Fract Eng Mater Struct. 2008;31:340–5.
[12] Li M, Maskill S, Wen Z, Yue Z, Sun W. A miniaturized thin-plate low cycle fatigue test method at elevated temperature. Fatigue Fract Eng Mater Struct. 2022;45:1361–78.
[13] Tomasz T, Janusz S, Przemysław S. Verification of methods used for fatigue testing of small steel specimens taken from existing structures. Solid State Phenom. 2016;250:232–7.
[14] Volak J, Novak M, Kaiser J, Mentl V. Fatigue testing by means of miniature test specimens. J Achiev Mater Manuf Eng. 2012;55(2):386–9.
[15] Furuya Y, Nishikawa H, Hirukawa H, Nishikawa H, Takeuchi E. Data sheets on fatigue properties of SUS304 (18Cr-8Ni) stainless steel bars for machine structural use, NRIM fatigue data sheet, No. 33. Tokyo: National Research Institute for Metals; 1983.
[16] Nagashima N, Nishikawa H, Hirukawa H, Takeuchi E, Furuya Y. Data sheets on long-term, high temperature low-cycle fatigue properties of SUS310S (25Cr-20Ni) hot rolled stainless steel plate, NIMS fatigue data sheet, No. 100. Tsukuba: National Institute for Materials Science; 2006.
[17] He L, Akebono H, Kato M, Sugeta A. Fatigue life prediction method for AISI 316 stainless steel under variable-amplitude loading considering low-amplitude loading below the endurance limit in the ultrahigh cycle regime. Int J Fatigue. 2017;101:18–26.
[18] He L, Akebono H, Sugeta A. Effect of high-amplitude loading on accumulated fatigue damage under variable-amplitude loading in 316 stainless steel. Int J Fatigue. 2018;116:388–95.
[19] Schijve J. Fatigue of structures and materials. New York: Springer; 2009. p. 153–6.